Feasibility of Single Scan for Simultaneous Evaluation of Pulmonary Ventilation and Perfusion with Dual-Energy CT: An Experimental Study

Sae Rom Hong

Department of Medicine

The Graduate School, Yonsei University

Feasibility of Single Scan for Simultaneous Evaluation of Pulmonary Ventilation and Perfusion with Dual-Energy CT: An Experimental Study

Directed by Professor Hye-Jeong Lee

The Doctoral Dissertation
submitted to the Department of Medicine,
the Graduate School of Yonsei University
in partial fulfillment of the requirements for the
degree of Doctor of Philosophy

Sae Rom Hong

June 2015

This certifies that the Doctoral Dissertation of
Sae Rom Hong is approved.

Thesis Supervisor : Hye-Jeong Lee

Thesis Committee Member#1 : Byoung Wook Choi

Thesis Committee Member#2 : Hyo-Chae Paik

Thesis Committee Member#3 : Moo Suk Park

Thesis Committee Member#4 : Eun Jin Chae

The Graduate School
Yonsei University

June 2015

ACKNOWLEDGEMENTS

I would like to express my sincerest appreciation to the thesis committee members, Professor Byoung Wook Choi, Professor Hyo-Chae Paik, Professor Moo Suk Park, and Professor Eun Jin Chae for the time they have spared for me and the many professional advices they have provided that contributed greatly. Thank you from the bottom of my heart to my supervisor, Professor Hye-Jeong Lee, who has always been there to guide and inspire me.

Mom and Dad, thank you for being so supportive for me, I love you. And thank you my dearest friends, for always being there and sharing wonderful memories with me and encouraging to get through the difficulties. Last but not least, I appreciate the time I could spend away from everything I have, the opportunity to look back, the change to be thankful to every small thing, and friends who shared one of greatest experiences in my lifetime.

Thank you.

Sae Rom Hong

TABLE OF CONTENTS

LIST OF FIGURES

LIST OF TABLES

<ABSTRACT>

Feasibility of Single Scan for Simultaneous Evaluation of Pulmonary Ventilation and Perfusion with Dual-Energy CT: an Experimental Study

Sae Rom Hong

Department of Medicine
The Graduate School, Yonsei University

(Directed by Professor Hye-Jeong Lee)

Purpose: To evaluate the feasibility of simultaneous single scan of krypton ventilation and iodine perfusion using dual-energy CT (DECT).

Materials & Methods: The study was approved by institutional animal experimental committee. For 10 beagle dogs, we first made an airway obstruction and then, a pulmonary arterial occlusion after one week. For each animal model, 3 sessions of DECT (Single static scan at the end of 80% krypton ventilation without iodine enhancement [krypton CT], 80% krypton ventilation with iodine enhancement [mixed contrast CT], iodine enhancement after a 30-minute washout with O2 [iodine CT]) were performed. Krypton maps were made for krypton CT and mixed contrast CT, and iodine maps were made for mixed contrast CT and iodine CT. Two radiologists assessed the presence of krypton or iodine defects on

each map, and measured the overlay HU in the diseased segment and contralateral control segment. Results were compared between krypton maps of krypton CT and mixed contrast CT, and between iodine maps of iodine CT and mixed contrast CT using the Wilcoxon signed-rank test.

Results: In airway obstruction models, krypton defects were visually distinguishable only in the diseased segment on the krypton map of krypton CT, but not in mixed contrast CT. However, measured overlay HU values of the diseased segment (3.5 ± 1.4 and 39.9 ± 1.4, respectively) on krypton maps were significantly decreased compared to the contralateral segment (17.7 ± 2.6 and 46.3 ± 4.4, respectively) in both krypton CT and mixed contrast CT (P = 0.002 for both). In all pulmonary arterial occlusion models, iodine defects were noted in the diseased segment on the iodine map either from iodine CT or mixed contrast CT. In iodine maps of the pulmonary arterial occlusion model, measured overlay HU values were significantly lower in the diseased segment (9.51±4.72 and 13.78±4.49, respectively) than in the contralateral segment (86.7 ±10.4 and 90.2 ± 6.6, respectively) in both iodine CT and mixed contrast CT (P = 0.002 for both).

Conclusion: Although some qualitative limitations may exist, it might be feasible to analyze pulmonary ventilation and perfusion simultaneously using DECT.

Key words : krypton, ventilation, perfusion, pulmonary function, DECT

Feasibility of Single Scan for Simultaneous Evaluation of Pulmonary Ventilation and Perfusion with Dual-Energy CT: an Experimental Study

Sae Rom Hong

Department of Medicine
The Graduate School, Yonsei University

(Directed by Professor Hye-Jeong Lee)

I. INTRODUCTION

Multidetector computed tomography (MDCT) provides morphological information and is the first-line choice in evaluating lung disease. However, evaluation of lung perfusion and ventilation is also important, because the supply of the oxygen and exchange of the nutrient and waste are performed through the coordination of the perfusion and ventilation. If the balance of the ventilation and perfusion is broken, pulmonary function decreases.[1,2]

With recent advances in technique and hardware, dual-energy CT (DECT) is increasingly integrated into clinical practice.[3,4] Ventilation CT using inert radio-opaque xenon gas on DECT enables separation of xenon from lung tissue using a single imaging acquisition through the material decomposition theory. Xenon-enhanced ventilation imaging has potential

clinical applications in COPD, asthma, bronchiolitis obliterans, bronchial atresia, and planning of lung volume reduction surgery for patients with COPD and lung cancer.[5-12] The iodine-enhanced image or perfusion CT on dual-energy technique is currently used in the evaluation of pulmonary embolic disease and has potential application in the emphysema.[13-16]

Currently, for evaluation of both ventilation and perfusion using DECT, most commonly used technique is done by xenon ventilation scan followed by iodine enhanced scan after xenon wash-out interval.[17] However, this technique requires additional radiation exposure.[16] In comparison, MRI does not rely on ionizing radiation, but has limitations of longer imaging acquisition time, high cost, and lack of wide availability.[18] If simultaneous single scan for ventilation and perfusion imaging is available using DECT, the exam can be done with lower radiation exposure, no misregistration, and saving time. Besides, virtual noncontrast images are reconstructed without additional scanning of noncontrast imaging, further reducing radiation dose. However, simultaneous single scan of xenon-ventilation and iodine-enhancement is hard to perform because of the near-by atomic number (53-Iodine, 54-Xenon) showing similar radioactive characters.[19] Meanwhile krypton is less radio-opaque than xenon, but is nonetheless perceptibly radio-opaque gas, thus is feasible as an inhalation contrast medium.[20] Krypton, with atomic number of 36, might be distinguishable from iodine using material decomposition theory on DECT. Therefore, we studied to assess the feasibility of the simultaneous single scan of krypton ventilation and iodine perfusion through the experimental animal study.

II. MATERIALS AND METHODS

1. Animal Model

This experiment was approved by our Institutional Animal Experimental Committee and performed according to local animal care guidelines. 10 beagle dogs with average body weight of 10.0 kg were examined in the study. A 22-gauge intravenous catheter was placed in the cephalic vein for contrast administration, and it was connected with a three-way valve. Anesthesia was induced with intramuscular injection of medetomidine HCL (0.02 mg/Kg, Tomidin, Provet veterinary products, Turkey) and intravenous injection of tiletamine/zolazepam HCL (5mg/Kg, Zoletil, Virbac laboratories, Carros, France).

With 10 animals, we made an airway obstruction model first and performed DECT, and induced a pulmonary arterial occlusion model in the same animal after one week. In an airway obstruction model, we introduced a 6 Fr balloon wedge pressure catheter (Teleflex, Athlone, Ireland) of 110cm in length into the segmental bronchus with fluoroscopic guidance. After the placement of balloon catheter, animals were intubated with a polyethylene tube 6.5-mm in diameter (Mallinckordt, Athlone, Ireland) and moved to the CT room in a prone position. The average time from animal preparation to transfer to the CT room was 20 minutes. After the animal arrived in the CT room, deep anesthesia was maintained using isoflurane (Forane; Abbott Laboratories, North Chicago, IL) through a mechanical ventilator (Royal-77S; Royal

Medical, Seoul, Korea) without spontaneous respiration. To prevent a development of dependent atelectasis, positive end-expiratory pressure (PEEP) was used.

In a pulmonary arterial occlusion model, we dissected the neck and exposed the jugular vein. After selection of segmental pulmonary artery using a 5 Fr angled KMP catheter (Cook Europe, Limerick, Ireland), pulmonary occlusion was induced by an PTA balloon catheter (Submarine; Santa Rosa, CA, USA). After the induction of pulmonary occlusion, dissected neck was sutured with the catheter fixed on skin, and the animal was moved to the CT room. The average time from animal preparation to transfer to the CT room was 30 minutes. Anesthesia was the same as the airway obstruction model. On the day after the CT scan of pulmonary arterial occlusion model, animals were sacrificed to see if there is any abnormality in the lung parenchyma or secondary change of parenchyma followed by model induction.

2. CT Scan

All CT scans were performed by a second generation dual source dual energy CT (Somatom Definition FLASH; Siemens Medical Solutions, Forchheim, Germany). In both experimental models, same scanning protocols were used as follows. First, noncontrast CT of the chest was performed to check, adjust, and confirm the location of the tip of the balloon catheter, to selectively occlude the segmental bronchus or pulmonary artery in each model. Then, animals were ventilated using 80% krypton (a mixture of 80% krypton and 20% oxygen) for 3 minutes. A single static scan with dual energy technique that covered the entire thorax was performed at the end of krypton ventilation without contrast enhancement [krypton CT]. After the scan, animals were ventilated with 100% oxygen for 10 minutes for krypton wash-out. Then, after ventilation with 80% krypton for 3 minutes, a single static scan was performed at the end of krypton ventilation with iodine contrast enhancement [mixed contrast CT]. 5mL Iopamidol (300 mg/ml, Isovue; Bracco Diagnostics, Princeton, NJ) was injected at a rate of 1.5 mL/sec and followed by 5mL of 40% mixture of contrast, and finally 5mL of saline bolus chase. Image acquisition started 18 seconds after the initiation of the contrast injection. This delay time was determined through the preliminary test, aimed at the maximal enhancement of main pulmonary artery. After the scan, animals were ventilated with 100% oxygen for 30 minutes, and without krypton ventilation, repeated scan was performed with contrast enhancement using same contrast injection protocol [iodine CT] (Figure1).

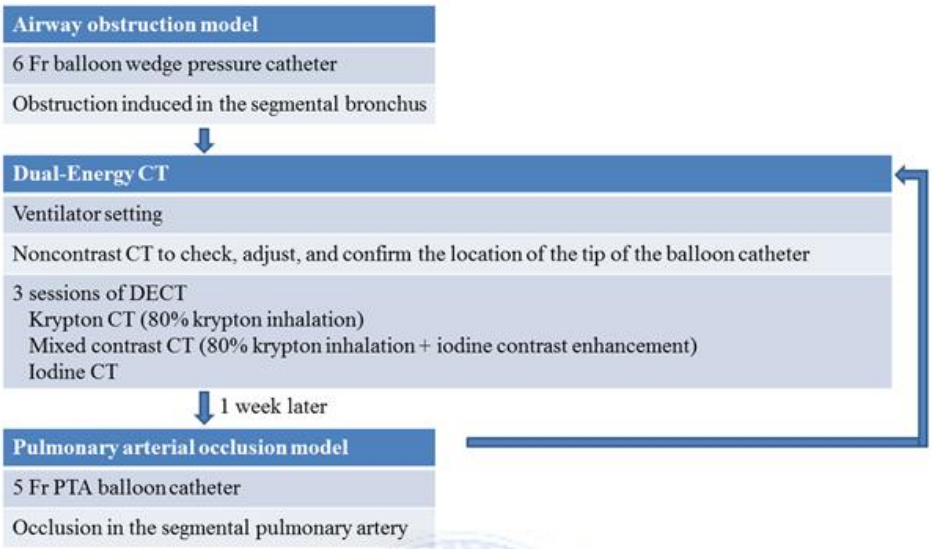

Figure 1. Diagram shows process of experiment.

3. Image Analysis

From the raw data of both detectors, images were reconstructed using a slice thickness of 0.6mm, an increment interval of 0.6mm, and a medium-smooth convolution kernel of D30. All CT images were transferred to a commercially available workstation (Syngo MMWP VE23A, Siemens Medical Solutions, Forchheim, Germany) for analysis. Two radiologists (S.R.H and H.J.L with 3 and 8 years of experience in chest CT interpretation, respectively) evaluated CT images including krypton maps (ventilation maps) and iodine maps (perfusion maps) in consensus reading. First, observers examined for motion artifacts and morphological abnormality of lung parenchyma including the secondary change according to bronchial obstruction or pulmonary artery occlusion on conventional CT images.

Afterward, krypton maps were obtained for images from krypton CT. Krypton maps were obtained at the workstation by using a modified prototype of the "Xenon" application class of the workstation, which was based on the material decomposition theory. We adjusted the material parameters for krypton extraction (Table 1).[21] Iodine maps were obtained for images from iodine CT. Iodine maps were obtained at the workstation by using a "Lung PBV" application of the workstation (Table 1). From the mixed contrast CT, both krypton maps and iodine maps were obtained. Finally two krypton maps and two iodine maps were made on fused images (50% of anatomical CT images and 50% of krypton or iodine images) with axial plane in each animal model.

Table 1. Adjusted material parameter for krypton and iodine extraction

	80kVp	140kVp
Krypton extraction		
Air	-995HU	-1000HU
Soft tissue	70HU	55HU
Krypton	-930HU	-970HU
Iodine extraction		
Air	-1000HU	-1000HU
Soft tissue	60HU	54HU

* Krypton extraction
Minimum value, −960 HU; maximum value, −500 HU; 4 for range
Contrast media cutoff value of -50HU
Pixels with densities outside of this range (below −960 HU and above −500 HU) set to 0 HU.
** Iodine extraction
Relative contrast material enhancement: 2.0
Minimum value, −960 HU; maximum value, −600 HU

For the qualitative assessment, we assessed the presence of color defects in the diseased segment and corresponding contralateral segment in each map. For the quantitative assessment, we placed circular regions of interest (ROI) on the site of obstructed or occluded segments and corresponding segments of the contralateral lung, by drawing while avoiding inclusion of airways and vessels in each map. The size and location of the ROI were kept constant for all images of both diseased segment and contralateral segment in each animal model. On each drawn ROI, overlay Hounsfield Unit (HU) values (DECT HU difference caused by krypton or iodine) were calculated.

4. Statistical Analysis

Statistical analysis was performed using software SPSS version 20 (SPSS, Inc., Chicago, IL, USA). Continuous variables were expressed as median ± interquartile range (IQR). Comparisons of overlay HU values were performed by using Wilcoxon signed-rank test. In krypton and iodine maps for both models, overlay HU values were compared between diseased segment and contralateral segment to see the difference of HU value made by obstruction/occlusion model (Figure 2). And overlay HU values in each diseased or contralateral segment for both models were compared between krypton map of krypton CT and krypton map of mixed contrast CT to see the overlay HU difference. Likewise, overlay HU values were compared between iodine map of iodine CT and iodine map of mixed contrast CT in each diseased or contralateral segment for both models. *P* values less than 0.05 were regarded as significant.

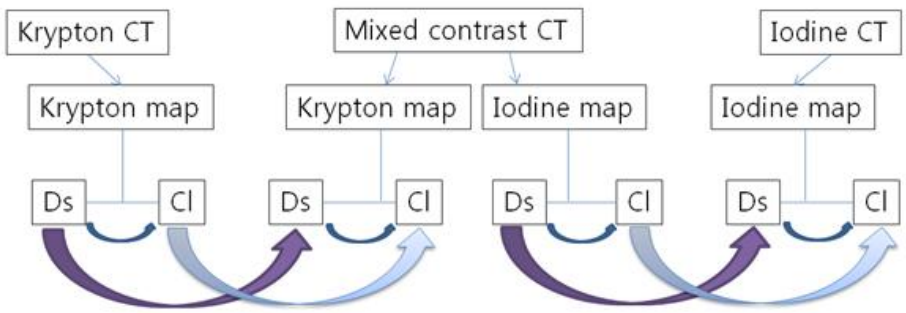

Figure 2. Diagram depicts comparisons performed between overlay HU values from krypton and iodine maps of three CT scans.

III. RESULTS

1. Qualitative assessment

The experimental model was successfully induced in all animals. On baseline noncontrast CT, the tip of the catheter was located to occlude the segmental bronchus or pulmonary artery which was randomly assigned during the procedure. Among all CT images, there were no excluded images from motion artifact or incidental parenchymal lesion. And there was no secondary change visualized on CT according to the bronchial obstruction or pulmonary arterial occlusion. In the histopathologic examination after completion of second CT scan, there was no parenchymal abnormality or secondary change following model induction.

In all airway obstruction models, krypton defect was noted in the diseased segment on the krypton map of krypton CT, but not in the contralateral segment. On the krypton map of mixed contrast CT, there was no visible krypton defect in both diseased segment and contralateral segment of all airway obstruction models, but decreased ventilation is just suspected in the diseased segment. There were no defects on iodine maps either from iodine CT or mixed contrast CT for airway obstruction model.

In all pulmonary arterial occlusion models, iodine defect was noted in the diseased segment on the iodine map either from iodine CT or mixed contrast CT but no iodine defects in the contralateral segments. In addition, no krypton defect was observed in both diseased and contralateral segments on the krypton maps either from krypton CT or mixed contrast CT.

2. Quantitative assessment

In all airway obstruction models, krypton defect was visually distinguished only in the diseased segment on the krypton map of krypton CT, but not in mixed contrast CT. However, measured overlay HU values of the diseased segment on krypton map were significantly decreased as compared to the contralateral segment in both krypton CT and mixed contrast CT (p = 0.002, p = 0.002, respectively). Meanwhile, extracted overlay HU values of krypton map from mixed contrast CT were significantly higher than those from krypton CT in both diseased segment and contralateral segment (p = 0.002, p = 0.002, respectively). In iodine maps of an airway obstruction model, there was no significant difference of the measured overlay HU values between the diseased segment and the contralateral segment in both iodine CT and mixed contrast CT (p = 0.348, p = 0.500, respectively).

In iodine maps of a pulmonary arterial occlusion model, measured overlay HU values were significantly lower in the diseased segment than in the contralateral segment in both iodine CT and mixed contrast CT (p = 0.002, p = 0.002, respectively). Extracted overlay HU values of iodine map from mixed contrast CT were higher than those from iodine CT in both diseased segment and contralateral segment, but the difference was not statistically significant (p = 0.061, p = 0.375, respectively). In krypton maps of a pulmonary arterial occlusion model, measured overlay HU values were not significantly different between diseased segment and contralateral segment in both krypton CT and

mixed contrast CT (p = 0.508, p = 0.111, respectively). However, when comparing overlay HU values of krypton CT to mixed contrast CT of the same segment, HU values from mixed contrast CT were significantly higher than those from krypton CT (p = 0.002, p = 0.002, respectively) (Table 2, 3).

Table 2. Results of functional parameter maps with krypton/iodine maps

		Diseased segment	Contralateral segment
Airway obstruction model	*Krypton map*		
	Krypton CT	5.55 (4.15 – 6.275)	15.65 (14.525 – 17.85)
	Mixed contrast CT	39.65 (37.45 – 44)	47.25 (42.225 – 49.3)
	Iodine map		
	Iodine CT	89.45 (85.7 – 95.6)	95.55 (80.675 – 98.15)
	Mixed contrast CT	91.55 (89.075 – 96.975)	94.2 (89.85 – 95.275)
Pulmonary arterial occlusion model	*Krypton map*		
	Krypton CT	17.35 (15.675 – 20.5)	16.35 (14.8 – 19.025)
	Mixed contrast CT	41.45 (39.475 – 45.025)	47.25 (42.225 – 49.3)
	Iodine map		
	Iodine CT	12.7 (11.575 – 18.75)	95.55 (81.425 – 100.175)
	Mixed contrast CT	19.1 (14.875 – 20.45)	93.5 (90.725 – 100.625)

Values are overlay HU value: median (interquartile range)

Table 3. Quantitative analysis using Wilcoxon signed rank test

		Difference between measured HU on maps		*p* value
Airway obstruction model	*Krypton map*	Krypton CT, Ds	Krypton CT, Cl	0.002
		Mixed contrast, Ds	Mixed contrast, Cl	0.002
		Krypton CT, Ds	Mixed contrast, Ds	0.002
		Krypton CT, Cl	Mixed contrast, Cl	0.002
	Iodine map	Iodine CT, Ds	Iodine CT, Cl	0.348
		Mixed contrast, Ds	Mixed contrast, Cl	0.5
		Iodine CT, Ds	Mixed contrast, Ds	0.138
		Iodine CT, Cl	Mixed contrast, Cl	0.461
Pulmonary arterial occlusion model	*Krypton map*	Krypton CT, Ds	Krypton CT, Cl	0.508
		Mixed contrast, Ds	Mixed contrast, Cl	0.111
		Krypton CT, Ds	Mixed contrast, Ds	0.002
		Krypton CT, Cl	Mixed contrast, Cl	0.002
	Iodine map	Iodine CT, Ds	Iodine CT, Cl	0.002
		Mixed contrast, Ds	Mixed contrast, Cl	0.002
		Iodine CT, Ds	Mixed contrast, Ds	0.061
		Iodine CT, Cl	Mixed contrast, Cl	0.375

Ds, Diseased model; Cl, Contralateral segment

IV. DISCUSSION

We aimed to see if simultaneous evaluation of ventilation and perfusion is feasible using DECT with krypton and iodine enhancement. So we designed experiment to see if there is a difference in analyzing krypton map and iodine map between those extracted from single scan of mixed contrast CT and each extracted from krypton CT or iodine CT separately. In our study, there was no qualitative or quantitative difference to distinguish diseased segment in iodine map extracted from mixed contrast CT as compared to iodine CT. However in krypton map, overlay HU values generally measured higher in mixed contrast CT than krypton CT. And though overlay HU value of diseased segment was significantly lower than HU value of contralateral segment in quantitative analysis, color defect was masked in qualitative analysis. In short, our study demonstrated that it is feasible to analyze pulmonary perfusion, but can be limited to analyze pulmonary ventilation using a single scan of mixed contrast CT with DECT.

In diagnosing or determining management of certain pulmonary diseases, assessment and quantification of pulmonary function are important.[22-25] In diseases involving small sized or peripheral airway or vessel, or in very early stages of disease, anatomical changes are so minute that diagnosis can be missed or delayed. Quantification using DECT can detect changes in small sized airway or vessels, and quantify ventilation or perfusion; thus aiding in diagnosis or stratify the patient's status.[25-27] With material decomposition theory of DECT, we can assess

pulmonary ventilation and perfusion by extracting inhalation gas or intravenous contrast medium.[28] But most commonly used scanning protocol requires separate scanning of ventilation and perfusion, causing increased exposure to radiation.[17,28] It is because the material decomposition method cannot differentiate most common inhalation gas – xenon – from iodine, because of nearby atomic number.[19] Besides, xenon can dissolve into blood making it even harder to differentiate from iodine which is injected into the blood vessel, and sometimes can show narcotic side effect. In contrast to xenon, krypton is much less soluble in tissue and therefore does not share the space with iodine making it easier to extract, and does not produce anesthetic effects.[20,29] Stefan *et al.* suggested feasibility of krypton as radiographic inhalation contrast media, showing less radiopaque than xenon, but nonetheless perceptibly radiopaque.[20] Moreover, because the atomic number of 36-Krypton is far from that of 53-Iodine, we hypothesized that material decomposition method can differentiate krypton and iodine from imaging dataset of DECT which is performed with krypton ventilation and iodine contrast enhancement at the same time.

Our study results showed that in analysis of mixed contrast CT, iodine analysis was not influenced by krypton, but krypton analysis was interfered by iodine. Overlay HU values of krypton extracted from mixed contrast CT were significantly higher than those from krypton CT in both disease segment and contralateral segment. And krypton defect seen in krypton map of mixed contrast CT was masked in krypton map of krypton CT. We assume the reason of this phenomenon can be inferred

from the principal of the material decomposition theory. The differentiation of material in CT is based on their X-ray attenuation. And attenuation is caused by absorption and scattering of radiation by the material under investigation. The two main mechanisms responsible for these effects are the Compton effect which is energy independent and Photo effect which is strongly energy-dependent. And CT numbers vary very much with beam energy for materials with higher atomic number. Thus, materials can be differentiated by applying different X-ray spectra and analyzing the differences in attenuation.[30] We think that because iodine has higher atomic number than krypton, iodine has bigger alteration of attenuation by changing photon energy. So in analysis of mixed contrast CT, krypton analysis is influenced by iodine having bigger attenuation difference, but there is little interference of krypton in analysis of iodine.

We expect that recent technique such as photon counting can be used to distinguish and quantify two materials in future work.[31,32]While DECT is performed using two x-ray spectra obtained at different tube voltages, photon counting obtains spectral measurements at different and relatively independent energies through the use of energy resolved detectors, which provides simultaneous measurements of the x-ray attenuation at multiple energies using standard polychromatic x-ray sources. But, major drawback of photon counting is limited detector speed, thus clinical application is not available yet.

Our study limitations are as follows. First, we used same animals twice each for airway obstruction model and pulmonary artery occlusion

model. But we used a balloon catheter to induce occlusion model which lasts only when the balloon is inflated. And we performed an airway obstruction model first which is less invasive and leaves no deformation, and had time gap of 1 week before a pulmonary arterial occlusion model. Second, histopathologic correlation for airway obstruction was not performed in this study. However, there was no specific abnormality or secondary change when reviewing the baseline noncontrast CT, or no abnormality was found in the histopathologic tissue after pulmonary arterial occlusion model induction. Third, although we studied animals without spontaneous respiration under deep anesthesia and each CT scan was performed during inspiratory plateau, a little anatomical difference could still be permissible when measuring CT numbers between images.

V. CONCLUSION

In conclusion, simultaneous evaluation of pulmonary ventilation and perfusion is feasible with a single scan of DECT using inert krypton and iodine enhancement. Visual and quantitative analysis of decreased ventilation and perfusion is distinguishable using color-coded maps. With further validation studies, we expect that DECT with krypton and iodine will be one-stop imaging modality giving virtual noncontrast imaging, ventilation, iodine maps along with detailed anatomical information.

REFERENCES

1. Cardus J, Burgos F, Diaz O, Roca J, Barbera JA, Marrades RM, et al. Increase in pulmonary ventilation-perfusion inequality with age in healthy individuals. Am J Respir Crit Care Med 1997;156:648-53.
2. Dantzker D, Brook C, Dehart P, Lynch J, Weg J. Ventilation-perfusion distributions in the adult respiratory distress syndrome. Am Rev Respir Dis 1979;120:1039-52.
3. Kaza RK, Platt JF, Cohan RH, Caoili EM, Al-Hawary MM, Wasnik A. Dual-energy CT with single-and dual-source scanners: current applications in evaluating the genitourinary tract. Radiographics 2012;32:353-69.
4. Ko JP, Brandman S, Stember J, Naidich DP. Dual-energy computed tomography: concepts, performance, and thoracic applications. J Thorac Imaging 2012;27:7-22.
5. Park E-A, Goo JM, Park SJ, Lee HJ, Lee CH, Park CM, et al. Chronic Obstructive Pulmonary Disease: Quantitative and Visual Ventilation Pattern Analysis at Xenon Ventilation CT Performed by Using a Dual-Energy Technique 1. Radiology 2010;256:985-97.
6. Chae EJ, Seo JB, Lee J, Kim N, Goo HW, Lee HJ, et al. Xenon ventilation imaging using dual-energy computed tomography in asthmatics: initial experience. Invest Radiol 2010;45:354-61.
7. Goo HW, Yu J. Redistributed regional ventilation after the administration of a bronchodilator demonstrated on xenon-inhaled dual-energy CT in a patient with asthma. Korean J Radiol 2011;12:386-9.
8. Goo HW, Yang DH, Hong S-J, Yu J, Kim B-J, Seo JB, et al. Xenon ventilation CT using dual-source and dual-energy technique in children with bronchiolitis obliterans: correlation of xenon and CT density

values with pulmonary function test results. Pediatr Radiol 2010;40:1490-7.

9. Goo HW, Yang DH, Kim N, Park SI, Kim DK, Kim EA-R. Collateral ventilation to congenital hyperlucent lung lesions assessed on xenon-enhanced dynamic dual-energy CT: an initial experience. Korean J Radiol 2011;12:25-33.
10. Zhang LJ, Zhou CS, Lu GM. Dual Energy Computed Tomography Demonstrated Lung Ventilation/Perfusion Mismatch in a 19-Year-Old Patient With Pulmonary Embolism. Circulation 2012;126:2441-3.
11. Yanagita H, Honda N, Nakayama M, Watanabe W, Shimizu Y, Osada H, et al. Prediction of postoperative pulmonary function: preliminary comparison of single-breath dual-energy xenon CT with three conventional methods. Jpn J Radiol 2013;31:377-85.
12. Zhang LJ, Zhou CS, Schoepf UJ, Sheng HX, Wu SY, Krazinski AW, et al. Dual-energy CT lung ventilation/perfusion imaging for diagnosing pulmonary embolism. Eur Radiol 2013;23:2666-75.
13. Chae EJ, Seo JB, Jang YM, Krauss B, Lee CW, Lee HJ, et al. Dual-energy CT for assessment of the severity of acute pulmonary embolism: pulmonary perfusion defect score compared with CT angiographic obstruction score and right ventricular/left ventricular diameter ratio. AJR Am J Roentgenol 2010;194:604-10.
14. Zhang L-J, Chai X, Wu S-Y, Zhao Y-E, Hu X-B, Hu Y-X, et al. Detection of pulmonary embolism by dual energy CT: correlation with perfusion scintigraphy and histopathological findings in rabbits. Eur Radiol 2009;19:2844-54.
15. Thieme SF, Becker CR, Hacker M, Nikolaou K, Reiser MF, Johnson TR. Dual energy CT for the assessment of lung perfusion-correlation to scintigraphy. Eur J Radiol 2008;68:369-74.

16. Kang M-J, Park CM, Lee C-H, Goo JM, Lee HJ. Dual-Energy CT: Clinical Applications in Various Pulmonary Diseases 1. Radiographics 2010;30:685-98.
17. Johnson T, Fink C, Schönberg SO, Reiser MF. Dual energy CT in clinical practice: Springer Science & Business Media; 2011.
18. Kauczor H-U, Hanke A, van Beek EJ. Assessment of lung ventilation by MR imaging: current status and future perspectives. Eur Radiol 2002;12:1962-70.
19. Goo HW. Dual-energy lung perfusion and ventilation CT in children. Pediatr Radiol 2013;43:298-307.
20. Winkler SS, Holden JE, Sackett JF, Flemming DC, Alexander SC. Xenon and krypton as radiographic inhalation contrast media with computerized tomography: preliminary note. Invest Radiol 1976;12:19-20.
21. Chung YE, Hong SR, Lee M-J, Lee M, Lee H-J. Krypton-enhanced ventilation CT with dual energy technique: Experimental study for optimal krypton concentration. Exp Lung Res 2014;40:439-46.
22. Pauwels RA, Buist AS, Calverley PM, Jenkins CR, Hurd SS. Global strategy for the diagnosis, management, and prevention of chronic obstructive pulmonary disease. Am J Respir Crit Care Med 2014;163.
23. Society AT. Idiopathic pulmonary fibrosis: diagnosis and treatment. International consensus statement. 2000.
24. Seo J, Im J, Chung J, Song J, Goo J, Park J, et al. Pulmonary vasculitis: the spectrum of radiological findings. Br J Radiol 2000;73:1224-31.
25. Hoeper MM, Barberà JA, Channick RN, Hassoun PM, Lang IM, Manes A, et al. Diagnosis, assessment, and treatment of non-pulmonary arterial hypertension pulmonary hypertension. J Am Coll Cardiol 2009;54:S85-S96.

26. Jobse BN, Rhem RG, Wang IQ, Counter WB, Stämpfli MR, Labiris NR. Detection of lung dysfunction using ventilation and perfusion SPECT in a mouse model of chronic cigarette smoke exposure. J Nucl Med 2013;54:616-23.
27. Han MK, Agusti A, Calverley PM, Celli BR, Criner G, Curtis JL, et al. Chronic obstructive pulmonary disease phenotypes: the future of COPD. Am J Respir Crit Care Med 2010;182:598-604.
28. Thieme SF, Hoegl S, Nikolaou K, Fisahn J, Irlbeck M, Maxien D, et al. Pulmonary ventilation and perfusion imaging with dual-energy CT. Eur Radiol 2010;20:2882-9.
29. Cullen SC, Gross EG. Additional Observations on Krypton'. Science 1951;113:580.
30. Johnson TR, Krauss B, Sedlmair M, Grasruck M, Bruder H, Morhard D, et al. Material differentiation by dual energy CT: initial experience. Eur Radiol 2007;17:1510-7.
31. Wang X, Meier D, Taguchi K, Wagenaar DJ, Patt BE, Frey EC. Material separation in x-ray CT with energy resolved photon-counting detectors. Med Phys 2011;38:1534-46.
32. Schlomka J, Roessl E, Dorscheid R, Dill S, Martens G, Istel T, et al. Experimental feasibility of multi-energy photon-counting K-edge imaging in pre-clinical computed tomography. Phys Med Biol 2008;53:4031.

Abstract (in Korean)

이중에너지 컴퓨터단층촬영을 이용한 폐 환기, 관류의 동시평가 가능성 연구

<지도교수 이 혜 정>

연세대학교 대학원 의학과

홍 새 롬

목적: 이중에너지 컴퓨터단층촬영(Dual-energy CT, DECT)을 이용하여 크립톤 환기와 아이오다인 관류를 한 번의 촬영으로 동시에 평가가 가능한지에 대하여 분석하여 알아보고자 한다.

대상 및 방법: 본 연구는 기관내 동물실험위원회의 승인하에, 10마리 비글에 폐 기관지 폐색유도와 1주일의 회복기 이후 폐세동맥 색전유도 실험을 진행하였다. 각 개체의 모델 유도후, 3번의 DECT (80% 농도의 크립톤 환기후 아이오다인 조영 없이 단일 정지영상 촬영 [크립톤 CT], 80% 크립톤 환기와 아이오다인 동시 조영 [혼합 조영 CT], 30분간 산소관류로 크립톤을 씻어낸 후 아이오다인 조영제만 사용하여 촬영 [아이오다인 CT]) 을 촬영하였다. 크립톤 CT와 혼합 조영 CT에서 크립톤 분포지도가 만들어지고, 혼합 조영 CT와 아이오다인 CT에서 아이오다인 분포지도가 만들어졌다. 두 명의 영상의학과 의사가 분포지도에서 크립톤과 아이오다인이 감소한 부위가 있는지를 평가하고 유도모델이 만들어진 분절과 반대측 대조군 분절에서 overlay HU

값을 측정하였다. 측정값은 Wilcoxon signed-rank test를 이용하여 크립톤 CT와 혼합 조영 CT에서 추출한 크립톤 분포지도끼리, 혼합 조영 CT와 아이오다인 CT에서 추출한 아이오다인 분포지도끼리 비교하였다.

결과: 폐기관지 폐색유도 실험에서, 크립톤 CT에서 추출한 크립톤 분포지도에서는 크립톤 감소가 육안으로 식별이 가능했으나, 혼합 조영 CT에서 추출한 크립톤 분포지도에서는 불가능했다. 그러나, 크립톤 분포지도에서 측정한 overlay HU 값은 크립톤 CT와 혼합 조영 CT 모두에서 폐색유도된 분절이 (3.5 ± 1.4 와 39.9 ± 1.4) 대조군 분절보다 (17.7 ± 2.6 와 46.3 ± 4.4) 유의하게 낮았다 (p = 0.002). 폐세동맥 색전 유도실험에서는, 혼합 조영 CT와 아이오다인 CT 모두에서 색전유도 분절에서 아이오다인 감소가 육안으로 식별가능하였다. 폐색전 유도실험의 아이오다인 분포지도에서 측정한 overlay HU 값은 혼합 조영 CT와 아이오다인 CT 모두에서 폐색유도된 분절이 (9.51±4.72 와 13.78±4.49,) 대조군 분절보다 (86.7 ±10.4 와 90.2 ± 6.6) 유의하게 낮았다 (p = 0.002).

결론: 정량분석에서의 한계점이 있으나, 이중에너지 컴퓨터단층촬영을 통해 폐환기와 관류를 한번의 촬영으로 동시에 평가할 수 있다.

핵심되는 말 : 크립톤, 환기, 관류, 폐기능, 이중에너지 컴퓨터단층촬영